SANS and XRR Porosimetry of a Polyphenylene Low-*k* Dielectric

Michael S. Silverstein*

Department of Materials Engineering, Technion-Israel Institute of Technology, Haifa 32000, Israel

Barry J. Bauer,* Ronald C. Hedden,† and Hae-Jeong Lee

Polymers Division, National Institute of Standards and Technology, Gaithersburg, Maryland 20899

Brian G. Landes

Dow Chemical Company, Midland, Michigan 48674

ABSTRACT: Nanometer scale porosity is introduced into low-dielectric constant ("low-*k*") materials to achieve permittivities less than 2.0. X-ray reflectivity (XRR) and small-angle neutron scattering (SANS) are complementary methods for characterizing pore size distributions (PSD). In this paper, the PSD in a polyphenylene low-*k* material is characterized via solvent vapor porosimetry experiments using both SANS and XRR to probe solvent permeation, and the significant differences in these techniques are described and discussed. Previous work assumed a single-mode PSD, but the solvent porosimetry measurements indicate the presence of a bimodal PSD. A PSD maximum is observed at about 5 Å via XRR porosimetry while SANS seems less sensitive to structure at high *q* (relatively small size scales). A sorption/desorption hysteresis suggests the presence of "ink-bottle" pores in which solvent-filled small pores block the desorption from large pores. A combination of these techniques is also able to describe the structure in a film with partially developed porosity that contains matrix, pores, and porogen.

Introduction

Nanometer scale porosity is introduced into low-*k* dielectrics to achieve permittivities of less than 2.0 that the *International Technology Roadmap for Semiconductors* indicates will be required for interlevel insulators in the near future.[1] It has proven extremely difficult to characterize the average pore size and pore size distribution in porous low-*k* dielectrics owing to the nanometer size scale of the pores. Materials under consideration for low-*k* dielectrics and characterization techniques used to determine their structures and properties have been reviewed recently.[2,3] The tandem of X-ray reflectivity (XRR) and small-angle neutron scattering (SANS) represents a powerful methodology for characterizing pore volume fraction (porosity) and pore size distribution in thin films.[4−9]

Nondestructive techniques used to investigate the pore size distribution in nanoporous low-*k* materials include ellipsometric porosimetry,[10−15] XRR porosimetry,[16−18] SANS porosimetry,[19−22] positronium annihilation lifetime spectroscopy (PALS),[23−25] small-angle X-ray scattering (SAXS),[26,27] and neutron reflectivity.[28] Ellipsometry, XRR, and PALS have been used to characterize a set of samples, yielding similar pore sizes, and the advantages and disadvantages of the techniques have been discussed in recent reviews.[13,29] The ellipsometric, XRR, and SANS porosimetry techniques are based on the phenomenon of adsorption and condensation in small pores. In solvent porosimetry, a porous film is exposed to a probe solvent vapor, and the solvent partial pressure is varied. Thermodynamically, the saturation vapor pressure of the vapor within a pore decreases with decreasing pore radius. Thus, the vapor within smaller pores will reach saturation at lower partial pressures than the vapor within larger pores. At these lower partial

pressures, the vapor will condense in the smaller pores, which become filled with liquid solvent, while the larger pores are filled with vapor.[30] The Kelvin equation (eq 1) relates the size of the pores that are filled with liquid to the partial pressure:

$$r = \frac{-2\gamma v_{\mathrm{m}}}{RT \ln(p/p_0)} \qquad (1)$$

where *r* is the pore radius, γ is the surface tension, v_{m} is the molar volume, *p* is the solvent vapor partial pressure, and p_0 is the saturated solvent vapor pressure.[30] Equation 1 assumes that pores are cylinders of infinite length. In a porosimetry experiment, solvent partial pressure is increased gradually from zero to p_0. The pores with the smallest radii (with the lowest saturated vapor pressure) fill with liquid solvent first, followed by pores of progressively larger radii, until all pores are filled at $p = p_0$.

Several experimental methods have been used to quantify solvent permeation in porosimetry experiments, and each technique relies on a different physical principle for solvent detection. Ellipsometric porosimetry uses a solvent whose refractive indices are known. XRR porosimetry uses a solvent whose electron density is known. SANS porosimetry uses a contrast match point solvent (MPS), a solvent whose neutron scattering length density (SLD) is the same as that of the matrix. The change in the refractive indices (ellipsometric porosimetry), the increase in the electron density (XRR porosimetry), or the decrease in the intensity of the coherent neutron scattering intensity (SANS porosimetry) is ascribed to solvent condensation in the pores. This paper characterizes the pore size distribution of a polyphenylene low-*k* dielectric with either fully developed or partially developed porosity using a combination of SANS porosimetry and XRR porosimetry. The significant differences between the two techniques are described and discussed.

† Present address: Department of Materials Science and Engineering, Penn State University, University Park, PA 16802.
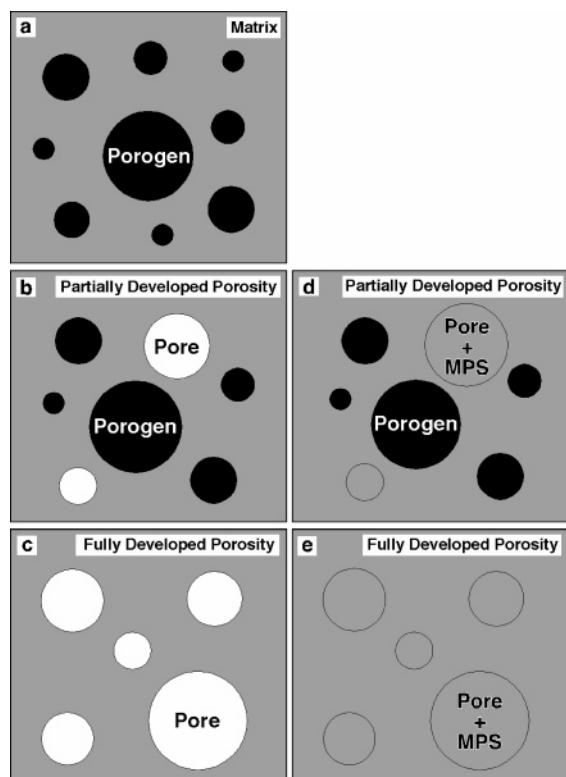* Corresponding authors. E-mail: michaels@tx.technion.ac.il, barry.bauer@nist.gov.

Figure 1. Schematic illustrations showing (a) 150A, (b) 400A, (c) 43040A, (d) 400A exposed to MPS, and (e) 43040A exposed to MPS.

Experimental Section

Materials. The solvents used were methanol (CH_3OH), methanol-d_3 (CD_3OH), toluene (C_7H_8), and toluene-d_8 (C_7D_8) (Sigma-Aldrich). The porous organic low-*k* material especially prepared for this research was based on a developmental version (V7) of Dow Chemical's SiLK[47] polyphenylene precursor. Such materials have been described in detail elsewhere.[31−35] The samples in question contained a deuterated porogen that degrades completely at 430 °C. All the samples discussed here (150A, 400A and 43040A) underwent a bake at 150 °C for 24 h. Sample 150A did not undergo further processing. The sample whose porosity was developed completely, 43040A, was exposed to 430 °C for 40 min. The sample whose porosity was only partially developed, 400A, was heated to 400 °C and then cooled immediately. Heating to 400 °C was found to remove about 50% of the porogen.[31] The structures of 150A, 400A, and 43040A are illustrated schematically in parts a, b, and c of Figure 1, respectively. The polyphenylene matrix cures during heating, undergoing cross-linking and releasing CO.[35] The film thicknesses, measured using ellipsometry, were 1.215, 1.095, and 0.935 μm for 150A, 400A, and 43040A, respectively.[31]

The Kelvin equation (eq 1) will be applied to toluene using a surface tension of 28 mN/m, a molar volume of 107 cm^3/mol, and a temperature of 25 °C. It is important to note that the Kelvin equation does not apply for pore radii smaller than about 5 Å.[27] The molecular radius of toluene is ~3 Å.[6]

Small-Angle Neutron Scattering. The SLD of component i is $\rho_i\sigma_i$, where ρ_i is its mass density and σ_i is the total scattering length per unit mass defined by

$$\sigma_i = \frac{N_A \sum_j c_j b_j}{\sum_j c_j m_j} \qquad (2)$$

where c_j is the local molar concentration of a nucleus j, b_j is its scattering length, m_j is its molar mass, and N_A is Avogadro's number.

The scattering contrast between two materials is defined as the absolute value of the difference between their SLDs. For a two-phase blend in which each phase has a homogeneous atomic composition, the scattered intensity, $I(q)$, is proportional to the contrast between the two phases squared, regardless of sample morphology:

$$I(q) \propto (\rho_1\sigma_1 - \rho_2\sigma_2)^2 \qquad (3)$$

where q is the scattering vector, related to the scattering angle, $2\theta_s$, and the neutron wavelength, λ_N, by $q = (4\pi \sin \theta_s)/\lambda_N$.

The bulk densities and atomic compositions of the probe solvents were used to calculate their neutron scattering length densities in the condensed liquid phase. The SLDs calculated for CH_3OH and CD_3OH are -0.373×10^{-6} and 4.28×10^{-6} Å^{-2}, respectively. The SLDs calculated for C_7H_8 and C_7D_8 are 0.94×10^{-6} and 5.67×10^{-6} Å^{-2}, respectively. A SLD of 2.37×10^{-6} Å^{-2} was calculated for the polymer based on its density (1.18 g/cm^3) and composition ($C_{86}H_{56}O$).[31] A SLD of 5.67×10^{-6} Å^{-2} was calculated for the porogen based on its density (1.07 g/cm^3) and composition ($C_{98}H_{10}D_{88}$).[31] The polymer−porogen scattering contrast is 3.30×10^{-6} Å^{-2}, significantly greater than the polymer−pore scattering contrast of 2.37×10^{-6} Å^{-2}.

The small-angle neutron scattering was performed at the National Institute of Standards and Technology (NIST) Center for Neutron Research. A stack of seven films on silicon wafer substrates was placed inside a custom-built flow-through stainless steel scattering cell with quartz windows and a gas inlet and outlet. The SANS was performed on the 8 m NG1 instrument, with a wavelength spread of 12%, and on the 30 m NG7 instrument, with a wavelength spread of 11%. The high q range (0.013−0.091 Å^{-1}) SANS data were taken on the 8 m SANS using a wavelength of 6 Å, the mid q range (0.005−0.051 Å^{-1}) data were taken on the 8 m SANS using a wavelength of 12 Å, and the low q range (0.002−0.027 Å^{-1}) data were taken on the 30 m SANS using a wavelength of 6 Å. Fits of the scattering data were made using a least-squares method, yielding standard deviations to the fit parameters.

X-ray Reflectivity. Specular X-ray reflectivity measurements (XRR) were performed using a modified Philips high-resolution X-ray diffractometer equipped with an environmental control chamber with Be windows. Data were collected at the specular condition, with the grazing incident angle, θ_i, equal to the detector angle, θ_d. The reflected intensity was recorded as a function of angle. XRR measurements were performed both under vacuum and in the presence of saturated solvent vapors, which condense in the pores. Both methanol and toluene were used as adsorbents, since they were expected to have quite different solubilities in the film. The magnitude of the momentum transfer in the film thickness direction, q_z, is related to θ_i and the wavelength of the Cu Kα_1 radiation (1.54 Å), λ_X, by $q_z = (4\pi \sin \theta_i)/\lambda_X$. The data were plotted as the log of the relative intensity (reflected beam intensity, I, divided by the incident beam intensity, I_0) vs q_z. The average electron densities of the films were deduced using a computer modeling routine (mlayer) capable of simulating reflectivity from multilayer structures.[36]

SANS and XRR Porosimetry. The solvent porosimetry technique used for SANS and XRR measurements uses dry nitrogen as a carrier gas. A stream of dry nitrogen is mixed with a stream of nitrogen saturated with solvent vapor to achieve the desired solvent partial pressure; the mixed stream is then passed over the sample. The ratio of the solvent-saturated nitrogen feed to the total nitrogen feed is the relative pressure of the solvent, p/p_0. Mass flow controllers were used to control the flow rates of dry nitrogen and of solvent-saturated nitrogen. Detailed descriptions of the experimental setups for SANS and XRR porosimetry have been published elsewhere.[17,19] For sorption (filling the pores), the relative pressure of the solvent was varied from 0 to 1. For desorption (emptying the pores), the relative pressure of the solvent was varied from 1 to 0.

The relative uncertainties of the data presented are estimated as one standard deviation of the mean. The total combined uncertainties from all external sources are not reported, as comparisons are
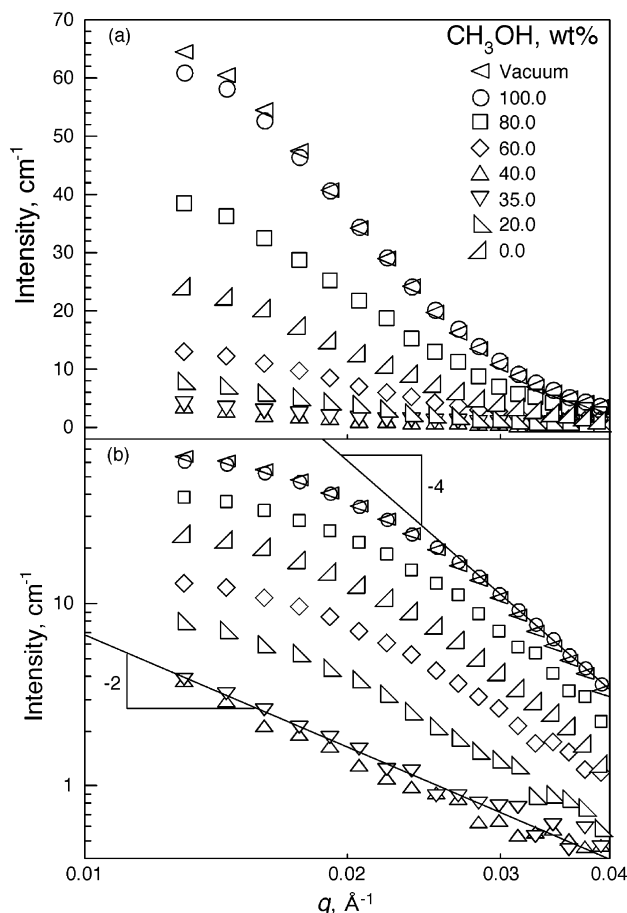
Figure 2. SANS data (8 m, 6 Å) from 43040A in the presence of various mixtures of CH_3OH and CD_3OH: (a) semilog; (b) log−log.

made with data obtained under the same conditions. In cases where the limits are smaller than the plotted symbols, the limits are left out for clarity. All temperatures reported are within ± 1 °C, thicknesses are within ± 1 nm, q_c^2 within $\pm 1 \times 10^{-5}$ Å^{-2}, and densities and porosities within $\pm 3\%$, as determined by previous experience of repeated measurements. The standard deviations from fits of the SANS data using a polydisperse hard-sphere model were less than $\pm 2\%$ for radius, $\pm 3\%$ for polydispersity, and $\pm 0.5\%$ for scattering contrast. The mass fractions are presented as weight percent (wt %).

Results and Discussion

Completely Developed Porosity: Determining the Methanol Match Point Solvent Composition. The SLDs of solvent 1 and solvent 2 are used to calculate the matrix match point solvent composition by solving eq 4 for the mole fraction of solvent 1, x_1.

$$x_1 = \frac{\rho_p \sigma_p - \rho_2 \sigma_2}{\rho_1 \sigma_1 - \rho_2 \sigma_2} \qquad (4)$$

where $\rho_p \sigma_p$, $\rho_1 \sigma_1$, and $\rho_2 \sigma_2$ are the SLDs of the polymer matrix, solvent 1, and solvent 2, respectively. Solving eq 4 for a mixture of CH_3OH and CD_3OH yields a mole fraction of 0.411 CH_3OH (a mass fraction of 0.390 CH_3OH).

The SANS scattering curves for 43040A exposed to the saturated vapors of various mixtures of CH_3OH and CD_3OH are seen in Figure 2 (the compositions are presented in terms of the weight percent CH_3OH). The highest scattering intensity is seen for vacuum conditions, and the scattering intensity is slightly lower for exposure to 100% CH_3OH vapor (although it
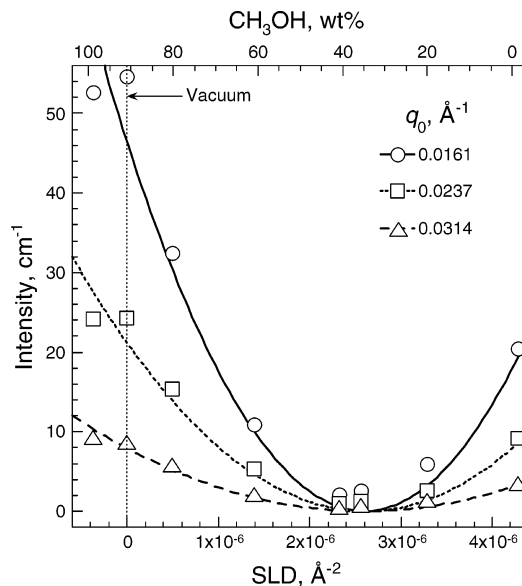

Figure 3. SANS intensities from 43040A in Figure 2 for q_0 of 0.0161, 0.0237, and 0.0314 Å^{-1} as a function of the solvent mixture (CH_3OH and CD_3OH) SLD and composition. Data from SANS in a vacuum, an SLD of zero, are also included. Quadratic fits to the data are used to find the SLD of the match point solvent mixture.

was expected to be slightly higher, a small discrepancy which may reflect experimental error). The scattering intensity in a vacuum scales as q^{-4} for q above 0.02 Å^{-1} and exhibits the very beginning of a plateau at a q of about 0.01 Å^{-1}. The scattering intensity decreases as the mass fraction of CD_3OH is increased. The scattering intensity reaches a minimum at about 40 wt % CH_3OH and then increases with further increases in the CD_3OH concentration. The scattering intensity for exposure to pure CD_3OH lies between the curves for exposure to 80 and 60 wt % CH_3OH. The scattering intensity is relatively small on exposure to 40 wt % CH_3OH. This minimum in scattering intensity with solvent composition occurs close to the calculated match point composition of 39 wt % CH_3OH.

The scattering intensity at a given q varies as the difference in SLDs squared (eq 3). The SLD of a mixture of CH_3OH and CD_3OH can be calculated from the component SLDs and the mole fractions in the mixture. Plotting $I(q)$ vs solvent SLD (as well as solvent composition) for 43040A at specific (arbitrarily selected) values of q, q_0, of 0.0161, 0.0237, and 0.0314 Å^{-1} yields the set of parabolas in Figure 3. The data in Figure 3 include the results from SANS in a vacuum since vacuum corresponds to a "solvent" SLD of zero.

The SLD of the match point solvent can be determined by fitting the data for each q_0 to eq 5.

$$I(q_0) = a(\rho_m \sigma_m - \rho_{MPS} \sigma_{MPS})^2 \qquad (5)$$

where $\rho_m \sigma_m$ is the SLD of the solvent mixture, $\rho_{MPS} \sigma_{MPS}$ is the SLD of the match point solvent from which the composition of the match point solvent can be calculated, and a is a fitting parameter. The fits to eq 5 yield match point SLDs of 2.60×10^{-6}, 2.62×10^{-6}, and 2.60×10^{-6} Å^{-2} or 34.1, 33.8, and 34.1 wt % CH_3OH for q_0 of 0.0161, 0.0237, and 0.0314 Å^{-1}, respectively. The average of 34.0 wt % CH_3OH is close to the match point composition of 39.0 wt % CH_3OH calculated using eq 4 for M-MPS (methanol match point solvent).

Scattering curves for 43040A in a vacuum and 43040A exposed to 35 wt % CH_3OH are compared in Figure 4. The data for 43040A in a vacuum are taken from the high, middle, and
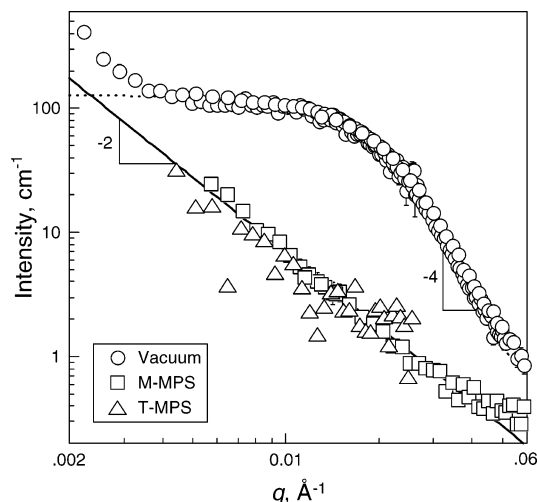
Figure 4. Comparison between SANS data from 43040A in a vacuum, SANS data from 43040A exposed to M-MPS (methanol match point solvent), and SANS data from 43040A exposed to T-MPS (toluene match point solvent). The solid line is a fit to the data from 43040A exposed to M-MPS, and the dotted line is the PHS fit to the data from 43040A in a vacuum.

low q ranges. The data for 43040A exposed to 35 wt % CH_3-OH are taken from the high and middle q ranges. The scattering in pure nitrogen (not shown) is the same as the scattering in a vacuum. The scattering in a vacuum clearly exhibits a plateau for q less than 0.01 Å^{-1}. At very low q, the scattering intensity begins to increase with decreasing q. A polydisperse hard-spheres (PHS) structural model was used to describe the scattering in a vacuum.[31,37,38] The PHS model provided a reasonable description of the SANS scattering. The variables in the PHS model include the volume fraction of the scattering phase, the scattering contrast, the average radius, the polydispersity, and the incoherent background. The volume fraction and scattering contrast are correlated, and therefore, one of them must be held constant on the basis of what is known about the material. The background is taken from the plateau in the scattering curves at the highest range of q measured. The resulting average pore radius of 80 Å was based on assuming a pore volume fraction of 0.12 from the XRR results.[31] The PHS model was not able to describe the scattering upturn at very low q, corresponding to a relatively large size scale.

In contrast, the scattering intensity for 43040A exposed to 35 wt % CH_3OH varies with q^{-2} throughout most of the q range measured, reaching a plateau (the background) at the highest range q measured (not shown). Systems that typically exhibit scattering that varies with q^{-2} include miscible polymer blends, blends without a two-phase structure. This scattering behavior indicates that when the pores are filled with 35 wt % CH_3OH, there is no discernible two-phase structure and no phase boundaries, as illustrated schematically in Figure 1e. The q^{-2} behavior arises from density fluctuations in the wall material. A linear fit to an Ornstein−Zernike plot ($1/I$ vs q^2) of the data from the mid q range for 43040A exposed to 35 wt % CH_3OH yields a fit correlation coefficient of 0.995. This confirms the q^{-2} relationship seen in Figure 4 and indicates that the correlation length describing the density fluctuations[39] is on the order of thousands of angstroms, larger than what can be measured quantitatively with the q range available.

It was not possible to find a reasonable fit to the SANS data for 43040A exposed to 35 wt % CH_3OH using the PHS model. The nature of the large-scale concentration fluctuations responsible for the scattering in 43040A exposed to 35 wt % CH_3OH

is unclear because the q range available was not adequate to characterize these features. One likely possibility is that there are long-range inhomogeneities in the wall SLD without any sharp interfaces or phase boundaries. In this case, the volume fraction of the scattering phase and its scattering contrast are not physically meaningful concepts, and therefore, little additional information could be offered by a PHS fit.

Partially Developed Porosity: Determining the Methanol Match Point Solvent Composition. Previous work has shown that there are significant differences between the film heated to 400 °C (400A) and the fully cured film that was held at 430 °C for 40 min (43040A). These differences are (a) 400A contains a significant amount of unpyrolyzed deuterated porogen and a relatively small pore volume fraction, (b) the volume fraction of pores in 400A (from solvent adsorption XRR) is about 0.05 (compared to 0.12 for 43040A), and (c) the SANS scattering intensity in a vacuum for 400A lies between that of the uncured porogen-filled film (150A) and that of 43040A. These differences indicate that 400A is partially developed, containing less porogen than the uncured film and more porogen than the fully cured film.[31] The scattering from the film prior to exposure to elevated temperatures (150A) was described by the PHS model using a porogen volume fraction of 0.26 (from the original composition) and a background scattering of 0.3 cm^{-1} (from the scattering data). The PHS fit yielded an average porogen domain radius of 60 Å, a polydispersity of 0.58, and a scattering contrast of 2.5×10^{-6} Å^{-2}.[31] The scattering from 43040A, fitted by assuming a pore volume fraction of 0.12 (solvent-sorption XRR) and a background scattering of 0.2 cm^{-1} (from the scattering data), was described by an average pore radius of 80 Å, a polydispersity of 0.38, and a scattering contrast of 1.7×10^{-6} Å^{-2}.[31] The difference between the porogen domain size distribution from 150A (a significant fraction of very small domains) and the pore size distribution from 43040A (no significant fraction of very small pores) was quite distinct.[31]

The SANS scattering curves for 400A exposed to the saturated vapors of various mixtures of CH_3OH and CD_3OH are seen in Figure 5 (the compositions are presented in terms of the mass percent of CH_3OH). Compared to the scattering from 43040A, the scattering from 400A is less sensitive to the composition of the vapor. The scattering intensities are the same for 400A exposed to vacuum and for 400A exposed to both 100 and 60 wt % CH_3OH vapor. The scattering intensity is slightly higher for 400A exposed to 80 wt % CH_3OH vapor. The lowest scattering intensity is seen for exposure to pure CD_3-OH vapor. The scattering from a polymer containing both pores and porogen is quite complex, but several conclusions can be drawn. The scattering is reduced on exposure to solvent vapor, and the extent of the reduction depends on the solvent's SLD. The fact that exposing 400A to a solvent does affect the scattering confirms that 400A contains pores that are being filled with solvent (the effects of swelling have been shown to be minimal).[31] The limited extent of the reduction in scattering in Figure 5 compared to the almost complete reduction in scattering in Figure 2 confirms that the polymer contains a significant amount of deuterated porogen and a relatively small amount of pores.

The presence of both deuterated porogen and pores makes it impossible to eliminate the scattering by filling the pores with a solvent. The extent to which 400A and 43040A are affected differently by exposure to various mixtures of CH_3OH and CD_3-OH can be seen by plotting $I(q)$ vs solvent SLD (as well as solvent composition) for 400A at specific (arbitrarily selected) q_0 of 0.0161, 0.0237, and 0.0314 Å^{-1} (Figure 6). Such plots
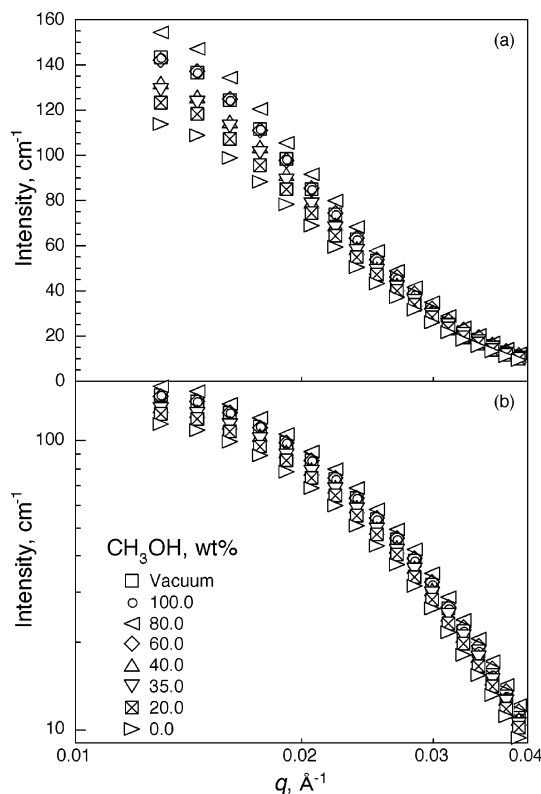
Figure 5. SANS data (8 m, 6 Å) for 400A in the presence of various mixtures of CH_3OH and CD_3OH: (a) semilog; (b) log−log.
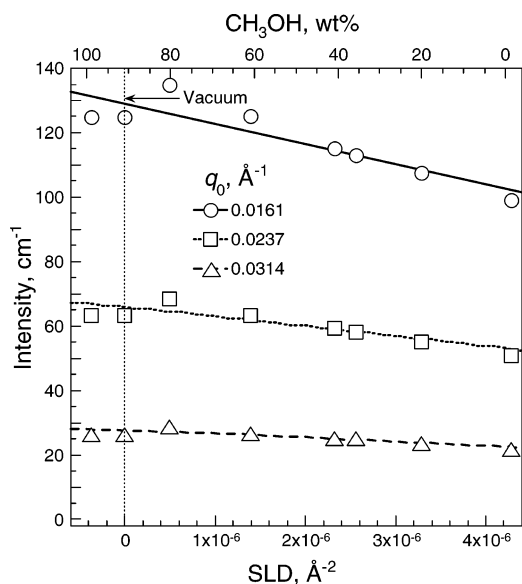

Figure 6. SANS intensities from Figure 5 for q_0 of 0.0161, 0.0237, and 0.0314 Å^{-1} as a function of the solvent mixture (CH_3OH and CD_3-OH) SLD and composition. Data from SANS in a vacuum, an SLD of zero, are also included. Linear fits are used as a visual aid.

for 43040A yield the set of parabolas seen in Figure 3. The same types of plots for 400A are described by a set of lines in Figure 6. For this three-phase system, the scattering decreases somewhat as the deuterium content of the solvent and, therefore, the solvent SLD increases.

It is reasonable to assume that the polymer matrix for 400A has approximately the same molecular structure and density as the polymer matrix for 43040A. Therefore, the match point composition for the matrix in 400A can be assumed to be similar to that for the matrix in 43040A. Therefore, when 400A is exposed to 35 wt % CH_3OH vapor, the pores are filled with a

liquid whose SLD matches that of the matrix. Under these circumstances, the three-phase system becomes a "two"-phase system as far as SANS is concerned, deuterated porogen surrounded by both polymer and by pores filled with 35 wt % CH_3OH, as illustrated schematically in Figure 1d. The PHS model can then be used to describe the porogen size distribution in 400A exposed to 35 wt % CH_3OH vapor.

The best fit to the PHS model, assuming a background scattering of 0.4 cm^{-1} (from the scattering data), yields an average radius of 59 Å, a polydispersity of 0.50, a volume fraction of 0.16, and a scattering contrast of 2.3×10^{-6} Å^{-2}. The polydispersity and scattering contrast are quite similar to the values found from the PHS fit to the scattering data for the porogen-filled film, 0.58 and 2.5×10^{-6} Å^{-2}, respectively. As opposed to the distinct difference between the porogen domain size distributions for 150A and the pore size distribution for 43040A, the porogen domain size distributions for 150A and 400A are almost identical. The porogen volume fraction is reduced from 0.26 in the original film to 0.16 in 400A. This reduction of 0.1 in the volume fraction of porogen corresponds in part to the pore volume fraction of 0.05 in 400A (solvent-sorption XRR).[31] Similarly, the entire porogen volume fraction of 0.26 becomes a pore volume fraction of 0.12 in 43040A.

It is shown here for the first time how completely independent measurements can be combined to follow the generation of pores by the pyrolysis of a porogen. The composition of the film prior to exposure to elevated temperatures was 74% oligomer matrix and 26% porogen. Solvent adsorption XRR has demonstrated that exposure to 400 °C yields about 5% porosity in the film while SANS in a vacuum indicates the presence of porogen as well.[31] As contrast match SANS indicates that there is 16% porogen in the film in addition to the 5% pores, this yields 79% matrix in the film. SANS in a vacuum has demonstrated that exposure to 430 °C for 40 min completely pyrolyzes the porogen, yielding a film with 88% matrix and 12% pores. This combination of techniques describes a consistent increase in the matrix fraction, from 74 to 88%, and is integral to the description of the pore formation mechanism in these materials.

Completely Developed Porosity: Methanol and Toluene Match Point Solvents. The SLDs of the toluene and deuterated toluene were used to calculate the toluene match point solvent (T-MPS) composition by solving eq 4 for x_1, yielding a mole fraction of 0.698 C_7H_8 (a mass fraction of 0.681 C_7H_8). The toluene composition used for SANS porosimetry was 68 wt % C_7H_8. On exposure to T-MPS, 43040A exhibited the scattering in Figure 4. The scattering for 43040A in the presence of T-MPS is quite similar to the scattering in the presence of 35 wt % CH_3OH (Figure 4). The similarity of the scattering on exposure of 4304A to 35 wt % CH_3OH or to T-MPS confirms that both solvent mixtures are indeed at the match point. In addition, this observation supports the idea that the SANS data reported here were not substantially affected by the choice of solvent, given that both the solvents used could penetrate the pores.

SANS Porosimetry. The effect of the T-MPS relative pressure on the scattering from 43040A was studied. Figure 7 exhibits scattering for relative pressures of 0, 0.5, 0.6, and 1. The changes in scattering were relatively small from vacuum to a relative pressure of 0.5, and the changes in scattering were almost negligible from a relative pressure of 0.6 to a relative pressure of 1.0. The exposure to T-MPS at a relative pressure of 0.5 yields a decrease in scattering which is especially significant at low q. The reduction in scattering intensity on increasing the relative pressure from 0.5 to 0.6 is more significant than the reduction in scattering intensity on increasing
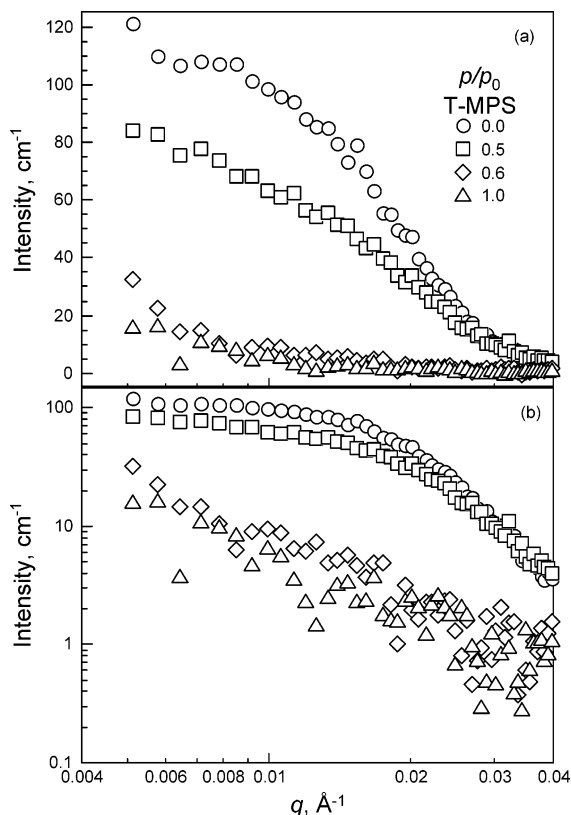
Figure 7. SANS data for 43040A at T-MPS relative pressures of 0, 0.5, 0.6, and 1: (a) semilog; (b) log−log.

the relative pressure from 0 to 0.5. The scattering reaches a minimum at a relative pressure of 0.6 and remains at that minimum with further increases in relative pressure.

The invariant, Q, is the quantity obtained when the scattering intensity is integrated over all directions. In the case of an isotropic material the invariant is

$$Q = \frac{1}{2\pi^2}\int_0^\infty q^2 I(q)\, dq \qquad (6)$$

In the case of an ideal two-phase system of pores in a matrix the invariant is

$$Q = V(\rho_1\sigma_1 - \rho_2\sigma_2)^2(\phi_2 - \phi_2^2) \qquad (7)$$

where V is the sample volume and ϕ_2 is the volume fraction of empty pores.[39] For low volume fractions of empty pores the variation of Q with ϕ_2 is close to linear. The 43040A pore volume fraction is relatively low. The pore volume fraction is 0.12 in a vacuum and is reduced with increasing relative pressure as the pores are filled with T-MPS. The invariant could, therefore, reflect pore volume fraction, assuming that the wall does not absorb solvent and produce an increase in wall density. Previous results have shown that the solvent appears to have a minimal effect on the wall density.[31]

To calculate the invariant exactly as in eq 6 requires extrapolation to q regions outside of the range of the collected data. Rather than attempting this, an invariant-like integral can be defined to describe the effects that the relative pressure has on the total measured scattering. This empirical measure differs from the invariant by not accounting for extremely large or small pores but is reported here to provide an additional measure of porosimetry. While it is limited to being an empirical measurement, it still provides qualitative information on pore filling that can be directly compared to XRR data. $C(p/p_0)$ for a given
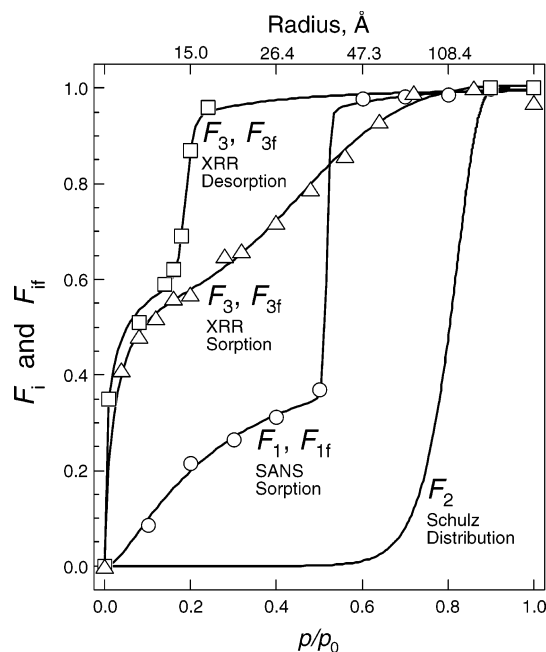

Figure 8. F_1 from SANS sorption porosimetry with T-MPS, F_2 from the Schulz distribution used to describe the results from SANS in vacuum, F_3 from XRR sorption/desorption porosimetry with toluene. The curves F_{1f} and F_{3f} describing the F_1 and F_3 data, respectively, are smooth fits using the sum of a sigmoidal function and a log−normal function. The corresponding radii are marked on the upper *x*-axis.

relative pressure is defined as the integral of $q^2 I$ for the data in Figure 7 (between 0.005 and 0.04 Å^{-1}, excluding very low q and very high q). $C(0)$ is the integral of $q^2 I$ when all the pores are empty. $C(1)$ is the integral of $q^2 I$ when all the pores are full. To more easily compare the results from SANS and XRR, it will be convenient to present $C(p/p_0)$ in normalized terms ranging from 0 (for $p/p_0 = 0$) to 1 (for $p/p_0 = 1$). F_1 in eq 8 is a simple normalization function that varies from 0 when all the pores are empty to 1 when all the pores are filled.

$$F_1 = \frac{C(0) - C(p/p_0)}{C(0) - C(1)} \qquad (8)$$

The variation of F_1 with the relative pressure is seen in Figure 8 (the corresponding radii are marked on the upper *x*-axis). There is a gradual increase in F_1 as the relative pressure increases from 0 to 0.5. F_1 increases rapidly from 0.35 at a relative pressure of 0.5 ($r = 35$ Å, eq 1) to 0.98 at a relative pressure of 0.6 ($r = 47$ Å). This relatively large increase in F_1 for a relatively small increase in relative pressure reflects the differences in the scattering curves in Figure 7 for relative pressures of 0.5 and 0.6. This suggests that the PSD contains a large fraction of pores of about the same size. The line through the data is a smooth fit function, F_{1f}, that uses the sum of a sigmoidal function and a log−normal function.[16]

The PHS Model. The PHS model used to describe the PSD from scattering in a vacuum assumes a single distribution peak described by the Schultz distribution in eqs 9 and 10.[40] The results from the PHS model fit to the SANS data for 43040A in a vacuum can be compared to the results from SANS porosimetry by formulating a cumulative volume fraction of pores filled based on $P(r)$ that is expressed in terms of the relative pressure. The cumulative volume fraction, F_2, which is expressed as a function of radius in eq 11, can be expressed in terms of relative pressure by applying the Kelvin equation (eq 1).

$$P(r) = \frac{1}{\Gamma(z+1)} \left(\frac{z+1}{R}\right)^{z+1} r^z \exp\left(-\left(\frac{z+1}{R}\right)r\right) \quad (9)$$

$$PD = \frac{1}{\sqrt{z+1}} = \frac{s}{R} \quad (10)$$

$$F_2 = \frac{\int_0^r P(r)r^3 \, dr}{\int_0^\infty P(r)r^3 \, dr} \quad (11)$$

where $P(r)$ is the probability distribution for r, R is the average radius, Γ is the gamma function, z is the width of the distribution, PD is the polydispersity, and s^2 is the variance of the distribution.

F_2 is also plotted in Figure 8. The differences in the shapes of the curves are obvious. One point of similarity between the F_1 and F_2 curves in Figure 8 is the relatively rapid increase in slope, seen for F_1 between relative pressures of 0.50–0.60 and for F_2 between relative pressures of 0.72–0.89. The increase in slope for F_2 occurs at an r of ~110 Å and reflects the long tail that the radius distribution exhibits at large radii.[31] The pores with large radii have a more pronounced effect on the average pore volume than on the average pore radius.

XRR Porosimetry. The variations in the XRR curves for 43040A exposed to different relative pressures of toluene can be seen in Figure 9. The critical edge, q_c, is the q_z value at the sharp drop in $\log(I/I_0)$ from the initially flat reflectivity curve. The electron density, and thus the mass density, is proportional to q_c^2. The q_c are 0.0216, 0.0218, and 0.0222 Å^{-1} for p/p_0 of 0, 0.02, and 1, respectively. As expected, q_c increases with increasing relative pressure since the number of pores that are filled with solvent increases and, therefore, so does the electron density.

It is useful to normalize the data in terms of the volume fraction of filled pores. The normalization function for XRR porosimetry, F_3 in eq 12, varies from 0 ($p/p_0 = 0$, all the pores are empty) to 1 ($p/p_0 = 1$, all the pores are filled). The F_3 from XRR sorption and desorption porosimetry are plotted in Figure 8. The lines through the data are from a smooth fit function, F_{3f}, that uses the sum of a sigmoidal function and a log–normal function.[16]

$$F_3 = \frac{q_c^2(0) - q_c^2(p/p_0)}{q_c^2(0) - q_c^2(1)} \quad (12)$$

The XRR porosimetry sorption–desorption cycle exhibits a hysteresis that is commonly found in ellipsometric, XRR, and SANS porosimetry of such nanoporous materials.[15,17,19,30] The hysteresis has been related to the presence of "ink-bottle" pores. An "ink-bottle" pore occurs in an open-pore arrangement in which pores with large radii are connected via constrictions, pores with small radii. When all the pores are filled with solvent, the desorption path for the large pores passes through the constrictions, the small pores. On decreasing the partial pressure, the desorption from the large pores should occur first, at higher partial pressures, while the smaller pores remain filled with liquid. However, the liquid in the small pore constrictions prevents desorption from taking place in the large pores. Desorption from the large pores occurs only when the small pores have undergone desorption, at significantly lower partial pressures.[15,41]

The F_3 sorption curve in Figure 8 exhibits a rapid increase between relative pressures of 0.0 and 0.20 ($r = 15$ Å). The rapid increase at low relative pressures is followed by a relatively
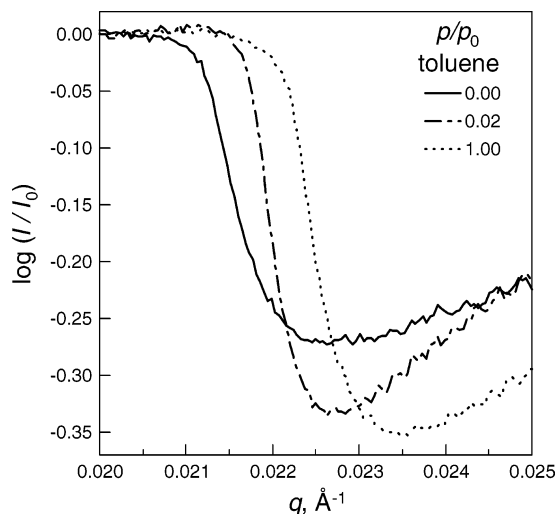

Figure 9. Variations in the XRR curves for 43040A exposed to toluene at relative pressures of 0, 0.02, and 1, exhibiting q_c of 0.0216, 0.0218, and 0.0222 Å^{-1}, respectively.
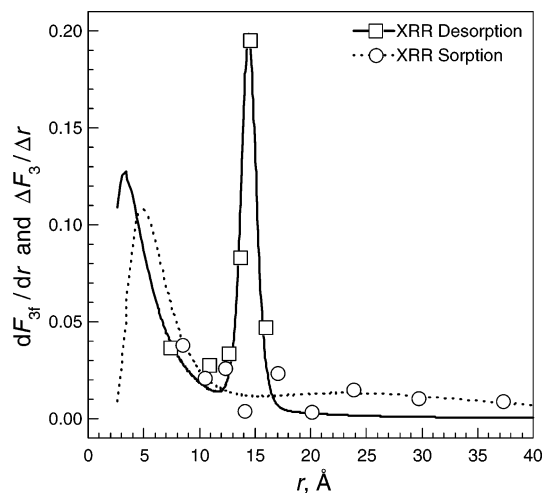

Figure 10. Pore size distributions based on Figure 8; dF_{3f}/dr and $\Delta F_3/\Delta r$ from XRR porosimetry sorption/desorption.

constant rate of increase until a plateau value of about 1.0 is reached at a relative pressure of 0.72 ($r = 74$ Å). The F_3 desorption curve remains at about 1.0 from a relative pressure of 1.0 until a relative pressure of 0.24 ($r = 17$ Å). Below a relative pressure of 0.24 there is a rapid decrease in F_3 that occurs in two stages. The first stage, between relative pressures of 0.24 and 0.14 ($r = 12$ Å), is the more rapid stage. The second stage, between relative pressures of 0.14 and 0.0, is more gradual and is very similar to XRR porosimetry sorption between relative pressures of 0.0 and 0.20.

Both the sorption and desorption data indicate the presence of two stages, with the initial sorption stage and the final desorption stage being almost identical. The presence of two stages in XRR porosimetry seems to confirm the existence of a bimodal pore size distribution. The existence of a bimodal distribution may be related to the "ink-bottle" pores that cause the sorption/desorption hysteresis. The smaller pores (from the peak at smaller radii) block desorption from the larger pores (from the peak at larger radii) until lower relative pressures are reached.

The bimodal pore size distribution curve from XRR porosimetry in Figure 10 is calculated by taking the derivative of F_{3f} (expressed in terms of r using eq 1) with respect to r, dF_{3f}/dr. The curves in Figure 10 are extrapolated to below 5 Å for

illustrative purposes only. The significant features below a radius of 5.25 Å in Figure 10 reflect the general behavior of the system. The data points from XRR porosimetry in Figure 10 are generated from the original data by dividing the increase in F_3 on increasing the relative pressure by the corresponding increase in radius, $\Delta F_3/\Delta r$.

The sorption and desorption curves in Figure 10 each indicate the presence of a bimodal distribution of pore sizes. There is a broad sorption peak at about 5 Å and broad desorption peak at about 3 Å. These peaks are similar in shape and position, reflecting the similarities in the sorption/desorption data between relative pressures of 0.0 and 0.2 in Figure 8. The relatively slow increase in F_3 for sorption at relative pressures above 0.2 is reflected in a very broad, small peak with a maximum at about 25 Å. The relatively rapid decrease in F_3 for desorption at relative pressures below 0.2 is reflected in a high, narrow peak with a maximum at about 14 Å. In general, the points derived from the experimental data seem to follow the curves generated from the derivatives of the curve fits.

The XRR sorption curve in Figure 8 is quite distinct from the SANS sorption curve. The differences between SANS sorption and XRR sorption may originate in the different sensitivities of the techniques to solvent sorption in the free volume of the matrix (including the pores generated by CO evolution during the curing reaction of the matrix).[35] The free volume radius for polyphenylene is about 3 Å.[42−44] The radii of the pores generated by porogen degradation are expected to be significantly larger. The polyphenylene matrix is cross-linked and has a high T_g, and therefore, it has a limited tendency to swell on toluene sorption.[31] The SANS curve based on the integral of q^2I from 0.005 to 0.04 Å^{-1} may neglect structures at high q, the relatively small size scale needed to characterize the pores with small radii seen in Figure 10. It is impossible to extrapolate to high q in order to supply the missing information owing to the variation of the integral with q^2I.[39] The PHS fit ignores any structure at relatively small scales and only describes the pore size distribution for large pores.

At very low relative pressures, toluene is sorbed into the matrix free volume, but not into the larger pores that are generated by porogen degradation. If there is no extensive swelling, the sorption of toluene by the matrix would produce an increase the electron density and thus an increase in the XRR q_c. The XRR porosimetry peak maxima of 3 and 5 Å in Figure 10 (corresponding to relative pressures between 0.0 and 0.20) are quite similar in size to the free volume radius of polyphenylene. SANS, however, is relatively insensitive to the extensive sorption/desorption at such low relative pressures. The sorption of T-MPS in the matrix free volume, on the other hand, may not yield a significant change in the neutron scattering since the scattering originates in the contrast between the matrix and the relatively large pores generated by porogen degradation. Similar results have been reported for nanoporous low-*k* materials based on a methylsilsesquioxane (MSQ) matrix.[45,46] For the nanoporous MSQ, XRR porosimetry yielded a bimodal distribution, distinguishing pores inherent in the matrix from pores generated by a porogen, the XRR sorption/desorption hysteresis yielded low, broad PSD peaks for sorption and high, narrow PSD peaks for desorption, and SANS was found to be less sensitive to the very small pores.

Conclusions

The pore size distribution in a nanoporous polyphenylene low-*k* material has been investigated using SANS contrast match solvent porosimetry and XRR porosimetry.

- The fully pyrolyzed film can be represented as a two-phase material, a uniform matrix, and pores accessible to a contrast match solvent. The match point solvent compositions were determined experimentally using a quadratic equation to describe the dependence of scattered intensity at arbitrarily chosen q_0 on composition. The experimentally determined match point solvent compositions for CH_3OH/CD_3OH (34 wt % CH_3OH) and C_7H_8/C_7D_8 (68 wt % C_7H_8) were close to those calculated from the elemental composition and density of the matrix.

- The partially pyrolyzed film containing matrix, pore, and porogen could not be matched with any solvent composition. Therefore, a three-phase system in which the matrix and residual porogen have sufficiently different SLDs can be easily distinguished from a two-phase system. The three-phase system was reduced to the equivalent of "two" phases (porogen surrounded by matrix and by solvent filled pores with the same contrast factor) through exposure to a contrast match solvent for the matrix. The porogen domain size distribution in 400A was similar to that in the original film. The film with partially developed porosity consisted of 5% pores (solvent absorption XRR), 16% porogen (contrast match SANS), and 79% matrix. This composition places it between the undeveloped film (74% matrix) and the film with fully developed porosity (88% matrix).

- The combination of SANS and XRR porosimetry produces more detailed information on the pore size distribution than either measurement alone. The relative insensitivity of SANS to structure in the high q region that corresponds to relatively small length scales makes pores in the smallest size ranges impractical to measure. XRR porosimetry accurately measures the amount of solvent uptake corresponding to small pore sizes and shows the existence of a bimodal pore size distribution that is quite different from the single peak PSD described by the PHS model.

- The sorption/desorption hysteresis suggests the presence of "ink-bottle" pores in which solvent-filled small pores block the desorption from large pores. This can complicate the determination of the true pore size distribution through porosimetry.

- The SANS scattering intensity from a fully pyrolyzed film exposed to a match point solvent varied as q^{-2}, indicating the existence of a single phase with large-scale concentration fluctuations in the matrix composition.

References and Notes

(1) *International Technology Roadmap for Semiconductors*, *2004 Update*; Semiconductor Industry Association: San Jose, 2004.
(2) Maex, K.; Baklanov, M. R.; Shamiryn, D.; Iacopi, F.; Brongersma, S. H.; Yanovitskaya, Z. S. *J. Appl. Phys.* **2003**, *93*, 8793.
(3) Maier, G. *Prog. Polym. Sci.* **2001**, *26*, 3.
(4) Bauer, B. J.; Lin, E. K.; Lee, H. J.; Wang, H.; Wu, W. L. *J. Electron. Mater.* **2001**, *30*, 304.

(5) Lee, H. J.; Lin, E. K.; Wu, W. L.; Fanconi, B. M.; Lan, J. K.; Cheng, Y. L.; Liou, H. C.; Wang, Y. L.; Feng, M. S.; Chao, C. G. *J. Electrochem. Soc.* **2001**, *148*, F195.

(6) Lee, H. J.; Soles, C. L.; Liu, D. W.; Bauer, B. J.; Wu, W. L. *J. Polym. Sci., Part B: Polym. Phys.* **2002**, *40*, 2170.

(7) Lee, H. J.; Soles, C. L.; Liu, D. W.; Bauer, B. J.; Wu, W. L. *Polym. Mater.: Sci. Eng.* **2002**, *87*, 435.

(8) Wu, W. L.; Wallace, W. E.; Lin, E. K.; Lynn, G. W.; Glinka, C. J.; Ryan, E. T.; Ho, H. M. *J. Appl. Phys.* **2000**, *87*, 1193.

(9) Silverstein, M. S.; Bauer, B. J.; Lee, H. J.; Hedden, R. C.; Landes, B.; Lyons, J.; Kern, B.; Niu, J.; Kalantar, T. In *Characterization and Metrology for ULSI Technology 2003, AIP Conference Proceedings*; Seiler, D. G., Diebold, A. C., Shaffner, T. J., McDonald, R., Zollner, S., Khosla, R. P., Secula, E. M., Eds.; AIP: New York, 2003; Vol. 683, p 572.

(10) Baklanov, M. R.; Mogilnikov, K. P.; Polovkinkin, V. G.; Dultsev, F. N. J. *J. Vac. Sci. Technol. B* **2000**, *18*, 1385.

(11) Shamiryan, D. G.; Baklinov, M. R.; Vanhaelemeersch, S.; Maex, K. *Electrochem. Solid-State Lett.* **2001**, *4*, F3.

(12) Murray, C.; Flannery, C.; Steiter, I.; Schulz, S. E.; Baklinov, M. R.; Mogilnikov, K. P.; Himcinschi, C.; Friedrich, M.; Zahn, D. R. T.; Gessner, T. *Microelectron. Eng.* **2002**, *60*, 133.

(13) Baklinov, M. R.; Mogilnikov, K. P. *Microelectron. Eng.* **2002**, *64*, 335.

(14) Mogilnikov, K. P.; Baklinov, M. R. *Electrochem. Solid-State Lett.* **2002**, *5*, F29.

(15) Baklinov, M. R.; Mogilnikov, K. P.; Yim, J. H. *Mater. Res. Soc. Symp. Proc.* **2004**, *812*, F5.4.1.

(16) Lee, H. J.; Soles, C. L.; Liu, D. W.; Bauer, B. J.; Lin, E. K.; Wu, W. L.; Grill, A. *J. Appl. Phys.* **2004**, *95*, 2355.

(17) Soles, C. L.; Lee, H. J.; Lin, E. K.; Wu, W. L. *Pore Characterization in Low-k Dielectric Films Using X-ray Reflectivity: X-ray Porosimetry*; NIST: Washington, DC, 2004.

(18) Lin, E. K.; Lee, H. J.; Lynn, G. W.; Wu, W. L.; O'Neill, M. L. *Appl. Phys. Lett.* **2002**, *81*, 607.

(19) Hedden, R. C.; Lee, H. J.; Bauer, B. J. *Langmuir* **2004**, *20*, 416.

(20) Hedden, R. C.; Bauer, B.; Lee, H. J. *Mater. Res. Soc. Symp. Proc.* **2003**, *766*, E9.7.1.

(21) Hedden, R. C.; Lee, H. J.; Soles, C. L.; Bauer, B. *Polym. Mater.: Sci. Eng.* **2004**, *90*, 494.

(22) Bauer, B. J.; Hedden, R. C.; Lee, H. J.; Soles, C. L.; Liu, D. W. *Mater. Res. Soc. Symp. Proc.* **2003**, *766*, E8.9.1.

(23) Gidley, D. W.; Frieze, W. E.; Dull, T. L.; Sun, J.; Yee, A. F.; Nguyen, C. V.; Yoon, D. Y. *Appl. Phys. Lett.* **2000**, *76*, 1282.

(24) Sun, J. N.; Gidley, D. W.; Dull, T. L.; Frieze, W. E.; Yee, A. F.; Ryan, E. T.; Lin, S.; Wetzel, J. *J. Appl. Phys.* **2001**, *89*, 5138.

(25) Ro, H. W.; Kim, K. J.; Theato, P.; Gidley, D. W.; Yoon, D. Y. *Macromolecules* **2005**, *38*, 1031.

(26) Huang, Q. R.; Volksen, W.; Huang, E.; Toney, M.; Frank, C. W.; Miller, R. D. *Chem. Mater.* **2002**, *14*, 3676.

(27) Omote, K.; Ito, Y.; Kawamura, S. *Appl. Phys. Lett.* **2003**, *82*, 544.

(28) Kim, H. C.; Volksen, W.; Miller, R. D.; Huang, E.; Yank, G.; Briber, R. M.; Shin, K.; Satija, S. K. *Chem. Mater.* **2003**, *15*, 609.

(29) Kondoh, E.; Baklanov, M. R.; Lin, E.; Gidley, D.; Nakashima, A. *Jpn. J. Appl. Phys.* **2001**, *40*, L323.

(30) Gregg, S. J.; Sing, K. S. W. *Adsorption, Surface Area and Porosity,* 2nd ed.; Academic Press: London, 1982.

(31) Silverstein, M. S.; Shach-Caplan, M.; Bauer, B. J.; Lee, H. J.; Hedden, R. C.; Landes, B. *Macromolecules* **2005**, *38*, 4301.

(32) Strittmatter, R. J.; Hahnfeld, J. L.; Silvis, H. C.; Stokich, T. M.; Perry, J. D.; Ouellette, K. B.; Niu, Q. J.; Godschalx, J. P.; Kalantar, T. H.; Mubarekyan, E.; Hefner, R. E.; Lyons, J. W.; Dominowski, J. M.; Buske, G. R. *Mater. Res. Soc. Symp. Proc.* **2003**, *766*, E7.5.1.

(33) Mohler, C. E.; Landes, B. G.; Meyers, G. F.; Kern, B. J.; Ouellette, K. B.; Magonov, S. In *Characterization and Metrology for ULSI Technology 2003, AIP Conference Proceedings*; Seiler, D. G., Diebold, A. C., Shaffner, T. J., McDonald, R., Zollner, S., Khosla, R. P., Secula, E. M., Eds.; AIP: New York, 2003; Vol. 683, p 562.

(34) Landes, B.; Kern, B.; Stokich, T.; Niu, J.; Yontz, D.; Radler, M.; Mohler, C. E.; Ouellette, K.; Lucero, S.; Hahnfeld, J.; King, D. *Mater. Res. Soc. Symp. Proc.* **2003**, *766*, E9.10.1.

(35) Martin, S. J.; Godschalx, J. P.; Mills, M. E.; Shaffer, E. O.; Townsend, P. H. *Adv. Mater.* **2000**, *12*, 1769.

(36) Ankner, J. F.; Majkrzak, C. F. In *Neutron Optical Devices and Applications, SPIE Conference Proceedings*; Majkrzak, C. F., Wood, J. M., Eds.; SPIE: Bellingham, WA, 1992; Vol. 1738, p 261.

(37) Griffith, W. L.; Triolo, R.; Compere, A. L. *Phys. Rev. A* **1986**, *33*, 2197.

(38) Griffith, W. L.; Triolo, R.; Compere, A. L. *Phys. Rev. A* **1987**, *35*, 2200.

(39) Roe, R. J. *Methods of X-Ray and Neutron Scattering in Polymer Science*; Oxford University Press: New York, 2000.

(40) Tuinier, R.; Petukhov, A. V. *Macromol. Theory Simul.* **2002**, *11*, 975.

(41) Ravikovitch, P. I.; Neimark, A. V. *Langmuir* **2002**, *18*, 1550.

(42) Simon, G. P.; Ardi, M. S.; Goodwin, A. A.; Zipper, M. D.; Andrews, S. R.; Shinton, G. W.; Galop, M.; Trimmer, M. *J. Polym. Sci., Polym. Phys.* **1998**, *36*, 1465.

(43) Marek, T.; Suvegh, K.; Vertes, A.; Ernst, A.; Bauer, R.; Weil, T.; Wiesler, U.; Klapper, M.; Mullen, K. *Radiat. Phys. Chem.* **2003**, *67*, 325.

(44) Suzuki, T.; Yoshimizu, H.; Tsujita, Y. *Polymer* **2003**, *44*, 2975.

(45) Lee, H. J.; Soles, C. L.; Liu, D. W.; Bauer, B. J.; Lin, E. K.; Wu, W. L. *Proc. IEEE Int. Interconnect Technol. Conf.* **2003**, 103.

(46) Lee, H. J.; Vogt, B. D.; Soles, C. L.; Liu, D. W.; Bauer, B. J.; Wu, W. L.; Lin, E. K. *Proc. IEEE Int. Interconnect Technol. Conf.* **2004**, 136.

(47) Certain commercial equipment and materials are identified in this paper in order to specify adequately the experimental procedure. In no case does such identification imply recommendation by NIST nor does it imply that the material or equipment identified is necessarily the best available for this purpose.